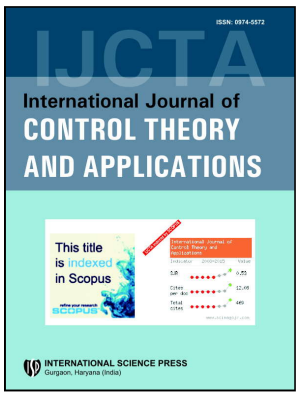

International Journal of Control Theory and Applications

ISSN : 0974-5572

Volume 10 • Number 6 • 2017

Heat Transfer Enhancement for a Trapezoidal Protruded Surface with Cross-flow Jet

Prateechee Padma Behera[1], Ashok K. Barik[2*], Ramesh K. Mallik[3]

[1] *Department of Mechanical Engineering* College of Engineering and Technology, Bhubaneswar-751029, Odisha, India,
Email: *prateechee24@gmail.com*
[2] *Department of Mechanical Engineering College of Engineering and Technology, Bhubaneswar-751029, Odisha, India,*
Email: *ashokbarik.mech@gmail.com*
[3] *Department of Mechanical Engineering College of Engineering and Technology, Bhubaneswar-751029, Odisha, India,*
Email: *rkmallik@cet.edu.in*

Abstract: In the present study, the conservation equations for mass, momentum and energy have been solved in a 3-D computational domain employing appropriate boundary conditions in ANSYS Fluent 16. SST $k-\omega$ model has been deployed to solve the turbulent kinetic energy and its specific dissipation. The nozzle and duct Reynolds number varied in the ranges of, $3,400 \le \mathrm{Re}_{\mathrm{Dh,nz}} \le 10,200$ and $17,900 \le \mathrm{Re}_{\mathrm{Dh,duct}} \le 53,900$. The Prandtl number of the fluid has also been varied in the range of $0.7 \le \mathrm{Pr} \le 15$. It has been observed that the heat transfer enhancement is a strong function of the duct Reynolds number and the Prandtl number of the fluid. The increment in the heat transfer rate is found to be insignificant over the range of the nozzle Reynolds number.

Keywords: Cross-flow, Jet Impingement, Prandtl Number, Turbulence.

1. INTRODUCTION

Now-a-days there is a growing demand for miniaturization of electronic devices. Various researchers [1–3] have investigated the thermal management of electronic devices. The thermal management of an electronic system and its performance are strongly related. As the technology advances, the circuit densities on a silicon chip continue to increase, the chips are packed in close proximity on multi-chip modules, and the power density continues to rise. But, the chip temperature must be maintained below $85\,^{0}$C. Since air has been used as a coolant in electronic systems due to its easy availability, low operational cost, so it has been widely used as a natural choice as an inexpensive coolant. The modification of the existing design of thermal equipment would be beneficial for heat transfer enhancement using air as a coolant. To dissipate heat effectively from a heated surface, several cooling strategies such as forced convective cooling, jet impingement cooling and the cooling by proving surface textures have been employed. Turbulators of various shapes such as transverse ribs [4-5], W-shaped ribs [6] and V-shaped ribs [7] have been proven to achieve an enhancement in heat transfer rate. The use of perforated ribs

also improves the heat transfer augmentation. The viscous sub-layer is disturbed by these perforations leading to a higher mixing of cold and hot fluids. For fully perforated baffles/ribs Karwa et al. [8] demonstrated that the Nusselt number is increased by 169%. Bhuiya et al. [9] reported that due to the presence of the perforated baffles the Nusselt number and friction factor were increased by 110–340% and 110–360%, respectively. Alamet al. [10] experimentally investigated the heat transfer augmentation by using V-shaped perforated blockages. The heat transfer rate in case of a perforated blockage was 33% higher than that of solid blockage. To investigate the heat transfer improvement Zhou and Feng [11] have used ribs of different shapes (rectangular, trapezoidal and delta).Various researchers [12-16] have shown that the heat transfer augmentation by jet impingement is an efficient and inexpensive method for cooling a heated surface. An efficient cooling strategy can be adopted for these devices to cater to the need for high processing speed, power density and uniform temperature. The temperature of the fluid in the vicinity of hot wall is higher than the temperature in other regions of fluid flow. If the cold fluid is carried and mixed with the hot fluid near the walls, the heat transfer rate is improved, thus lowering the temperature of the electronic chips. The creation of small-scale vortex pairs and exchange of momentum between jet and surrounding fluid by employing jet impingement method, can improve the heat transfer rate. Thus, the jet impingement method is found to be better than the forced convection method. In the present study, the heat transfer enhancement for protruded surface has been studied by varying duct Reynolds number, nozzle Reynolds number as well as the Prandtl number of the fluid. Although recently, Barik et al. [18] studied the heat transfer characteristics of a protruded surface using air as the working fluid, the effect of the Prandtl number on the heat transfer rate has not been studied by them. Thus, we derive our confidence to carry out the present study by varying the Prandtl number.

2. MATHEMATICAL MODELLING

2.1. Physical model and grid arrangement

In the present investigation, air has been used as the working fluid for the duct as well as the nozzle. A rectangular duct of size $0.67m \times 0.023m \times 0.03m$ has been used in the present study as shown in Fig. 1. Air enters inlet of the duct at velocity u_i and temperature T_{in}. To promote the heat transfer rate, a square nozzle impinges air on the main flow, forming a cross-flow with the main flow in order to impart a better mixing of hot and cold fluids. Four numbers of trapezoidal protrusions are installed on the bottom isothermal wall. The details of the protrusions are given in Fig. 1. The bottom surface of length X/Dh_{duct} = 5.76 is maintained at a constant temperature ($T_w = 353K$).

On the upstream of the hot surface an extra length of X/Dh_{duct} = 10 has also been considered to ensure a fully developed duct flow. Similarly, in order to minimise the backflow effects at the duct exit, an extra length of

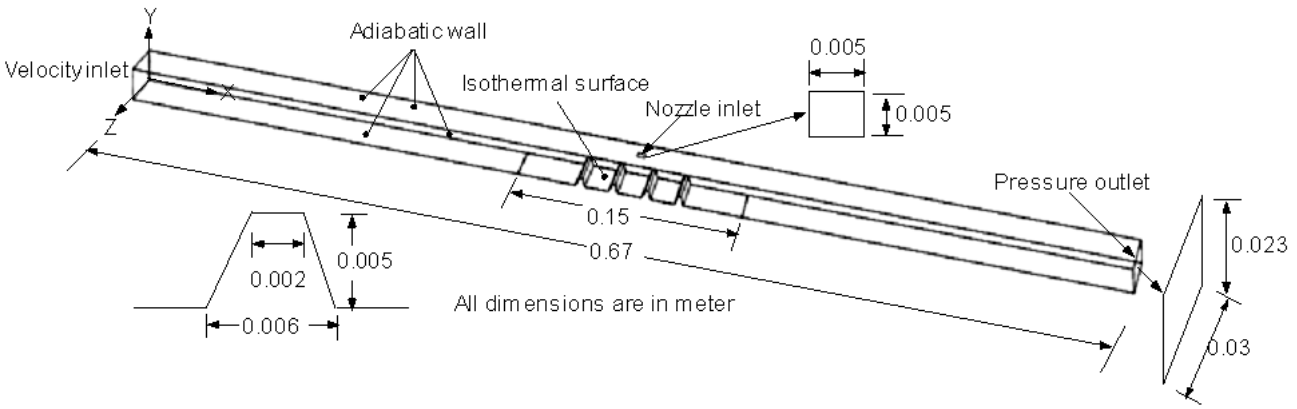

Figure 1: Schemetic computational domain with different boundary conditions.

X/Dh_{duct} = 10 has also been provided. The inlet and outlet of the main duct has been meshed with hexahedral cells. However, the nozzle inlet has been meshed with triangular cells due to the presence of inclined surfaces on the protrusions. The number of cells is relatively large at the nozzle inlet, duct inlet and the protruded surfaces. By doing this, one can capture the sharp gradient in flow variables on these surfaces. The mesh size has been controlled by applying rectangular cells at the duct walls other than the hot wall. The isothermal wall along with the surface protrusions have been meshed with triangular cells due to the presence of the inclined surfaces. The computational domain has been meshed with hexahedral as well as tetrahedral cells i.e. a hybrid meshing scheme (the combination of hexahedral and tetrahedral cells). The number of cells is controlled by hybrid meshing and the false diffusion (numerical diffusion) arising from the excessive number of cells is suppressed. The hydraulic diameters of the duct and nozzle are kept 0.02604 m and 0.005 m respectively throughout the investigation.

3. MATHEMATICAL FORMULATIONS

3.1. Governing differential equations

The Reynolds time-averaged equations for mass, momentum, energy in an inertial reference frame are written as follows:

Continuity equation:
$$\frac{\partial \overline{u_i}}{\partial x_i} = 0 \tag{1}$$

Momentum equation:
$$\overline{\rho u_i} \frac{\partial \overline{u_i}}{\partial x_i} = -\frac{\partial \overline{p}}{\partial x_i} + \frac{\partial}{\partial x_j}\left(2\mu \overline{S_{ij}} - \overline{\rho u_i' u_j'}\right) \tag{2}$$

Energy equation:
$$\overline{\rho u_j} \frac{\partial \overline{T}}{\partial x_j} = \frac{\partial}{\partial x_j}\left(\frac{\lambda}{c_p}\frac{\partial \overline{T}}{\partial x_i} - \overline{\rho u_i T'}\right) \tag{3}$$

The mean stain rate is defined as:
$$\overline{S_{ij}} = \frac{1}{2}\left(\frac{\partial u_i}{\partial x_j} + \frac{\partial u_j}{\partial x_i}\right) \tag{4}$$

Where μ, λ and c_p represent the dynamic viscosity, thermal conductivity and specific heat at constant pressure for the working fluid, respectively. The Reynolds stress ($-\rho \overline{u_i' u_j'}$) and turbulent heat flux ($-\rho \overline{u_i' T'}$) terms are appearing due to the time averaging, and these terms need to be closed by using the appropriate turbulence model. The Reynolds stress can be specified using a linear eddy viscosity model as follows:

$$-\rho \overline{u_i' u_j'} = 2\mu_t \overline{S_{ij}} - \frac{2}{3}\rho k \delta_{ij} \tag{5}$$

Where, k denotes the turbulent kinetic energy and μ represents the eddy viscosity, which are to be specified by solving the transport equations for the turbulent kinetic energy (k) and specific dissipation rate using the $k-\omega$ turbulence model. Similarly, the turbulent heat flux is defined as

$$-\rho \overline{u_i' T'} = \frac{\mu_t}{Pr_t}\frac{\partial \overline{T}}{\partial x_i} \tag{6}$$

Here, Pr_t denotes the turbulent Prandtl number. The SST $k-\omega$ turbulence model proposed by Mentor [17] is implemented in the present study so as to model the turbulence quantities. The governing equations for the

turbulence kinetic energy (k) and specific dissipation of turbulence kinetic energy (ω) can be seen from Ref. [18]. Different model constants used in SST $k-\omega$ turbulence model are given as follows:

$\alpha_{\infty}^{*}=1$, $\beta_{\infty}^{*}=0.09$, $\beta_i=0.072$, $\sigma_{k,1}=1.176$, $\sigma_{\omega,1}=2$, $\sigma_{k,2}=1$, $\sigma_{\omega,2}=1.168$, $R_k=6$, $a_1=0.31$ and $R_\beta=8$. The heat transfer coefficient is computed as follows:

$$h=\frac{Q}{A_{total}(T_w-T_\infty)} \tag{7}$$

$$A_{total}=A_{bw}+A_p \tag{8}$$

The total area (A_{total}) is the sum of the bare area of the heated surface (A_{bw}) and area of the surface protrusions (A_p).

The Nusselt number is computed as, $Nu=\frac{hL}{\lambda}$ (9)

3.2. Numerical solution procedure

Conservation equations for mass, momentum and energy are solved iteratively in a three-dimensional computational domain using the appropriate boundary conditions in ANSYS Fluent 16. The advection and diffusion terms are discretized using second order upwind and central difference schemes to yield a set of algebraic equations, which are then solved by the whole field residual method of ANSYS Fluent 16. SIMPLE (Semi-Implicit Method for Pressure Linked Equations) algorithm has been employed for pressure–velocity coupling to solve pressure correction equation. The convergence criterions for all the equations except the energy equation are set to be10^4. The convergence criterion for energy equation is set to 10^{-7}. In the present study, the SST (Shear Stress Transport) $k-\omega$ turbulence model has been used. It is worth to mention here that the SST $k-\omega$ model is more appropriate for modelling the flows which involve flow separation and reattachment due to the adverse pressure gradient. To model the principal stress through the SST $k-\omega$ turbulence model, the turbulent viscosity has been modified by incorporating the blending functions (i.e., F1 and F2) and the mean strain rate. Moreover, the blending functions in SST $k-\omega$ turbulence model effectively use $k-\omega$ model in the near-wall region as well as $k-\omega$ model in the far-field region. The addition of a cross diffusion term in $-\omega$ equation makes it suitable for both the near-wall and the far field regions. In the present study, the flow separation and its reattachment are expected because of the surface protrusions. Therefore, the SST $k-\omega$ model is preferred over the standard $k-\omega$ and $k-\omega$ models.

3.3. Boundary conditions

Air enters the computational domain through the nozzle and duct inlets at uniform velocity, so the velocity inlet boundary conditions have been imposed on the nozzle and duct inlets. The side and top surfaces (excluding the nozzle inlet) are taken as adiabatic wall. A constant temperature has been imposed on the heated bottom wall. The pressure outlet boundary condition is applied on the outlet because the outlet is assumed to be at ambient conditions. The mathematical descriptions of different boundary conditions are given as follows:

At adiabatic walls: $u=v=w=0$ and $\frac{\partial T}{\partial x}=\frac{\partial T}{\partial y}=\frac{\partial T}{\partial z}=0$ (10)

At solid isothermal wall: $u=v=w=0$ and $T=T_w=353\ K$ (11)

At duct inlet: $u = u_{in}, T = T_{\infty} = 300\ K$ (12)

At nozzle inlet: $v = -v_{in}, T = T_{\infty} = 300\ K$ (13)

Here *u, v* and *w,* are the velocity components in the X, Y, and Z-directions, respectively.

At pressure outlet: $p = p_{\infty}$ and $T = T_{\infty}$ (14)

Where, P_{∞} and T_{∞} are the ambient pressure and temperature, respectively. The turbulent intensity at duct and nozzle inlets are computed as, $I = 0.016\ Re^{-18}$ (15)

4. VALIDATION

The present numerical scheme has been validated with the experimental data of existing literature. However, the literature on heat transfer enhancement by cross flow jet and surface protrusions (i.e., the hybrid cooling scheme) is sparse. Thus, the present numerical scheme is validated with Sleicher and Rouse [19] correlation by taking a three-dimensional circular pipe of diameter 0.026 m and length 0.67 m, and applying a uniform wall heat flux (i.e. 100 W/m^2) to the fully developed portion of the duct.

This particular problem is chosen, since the boundary conditions for the validation purpose is similar to our present boundary conditions. A grid sensitivity test has also been carried out for the present validation, and it is found that a grid size of 28, 891 cells predicts the surface Nusselt number reasonably well with the above correlation as shown in Fig. 2. Moreover, the computed values of Nusselt number are close to the values predicted by Kakac et al. [20] correlation. For the above validation, SIMPLE method has been used for pressure-velocity coupling and the second order upwind scheme is used for solving mass, momentum and energy equations. The SST $k-\omega$ turbulence model has been used to solve the equations for the turbulent kinetic energy and its dissipation

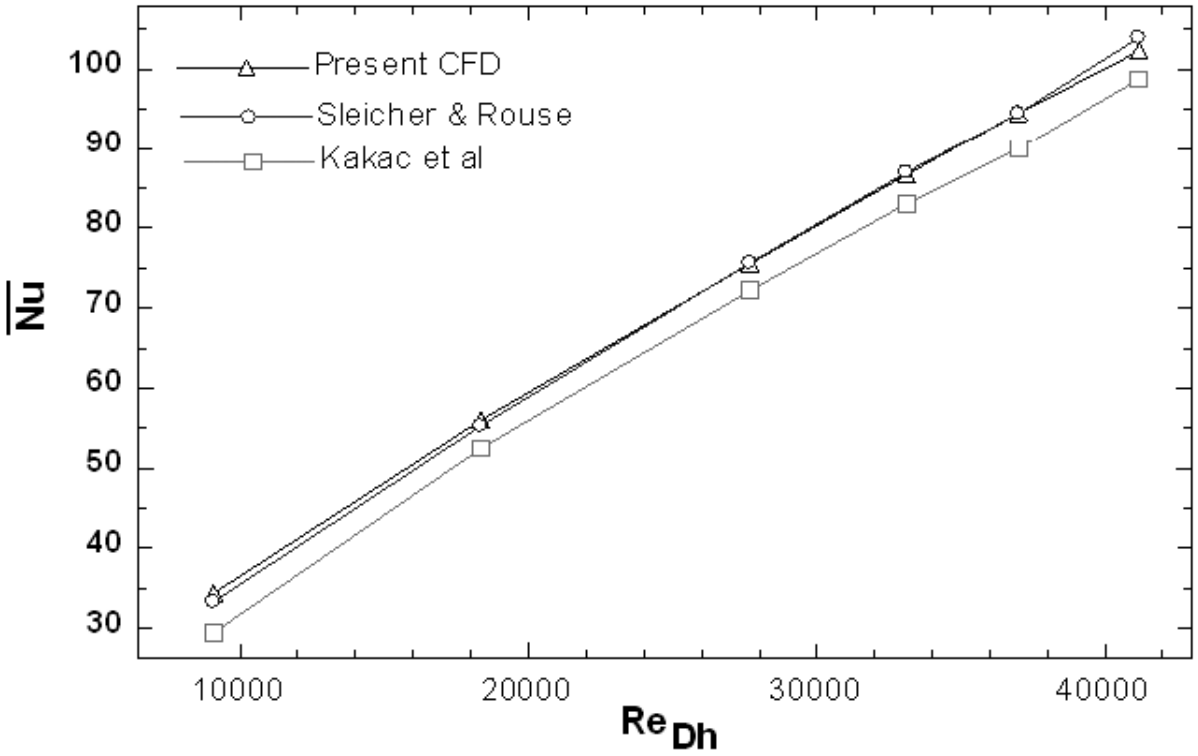

Figure 2: Variation of average Nusselt number with duct Reynolds number.

rate in the computational domain. It has been observed from Fig, 2 that the present numerical methodology is quite capable of computing the Nusselt number in the computational domain considered in the present study.

5. RESULTS AND DISCUSSIONS

5.1. Grid independence solution

The grid independence study has been carried out at duct and nozzle Reynolds number of 17,830 and 5,135, respectively. The variation of Nusselt number with the number of cells in the computational domain has been illustrated in Fig. 3. The number of cells in the computational domain has gradually increased from 78,000 to 244,000 cells so as to ensure that the area weighted average Nusselt number is independent of the Reynolds number. The computation has been started with 78,000 cells where the Nusselt number is found to be 74. A rapid increase in Nusselt number has been noticed as the number of cells is increased from 78,000 to 159,000. By doing this, the Nusselt number has been increased by 28.87%. Thereafter the increment in Nusselt number is insignificant. Thus, the computational domain with 159,000 cells is taken as the grid independent domain.

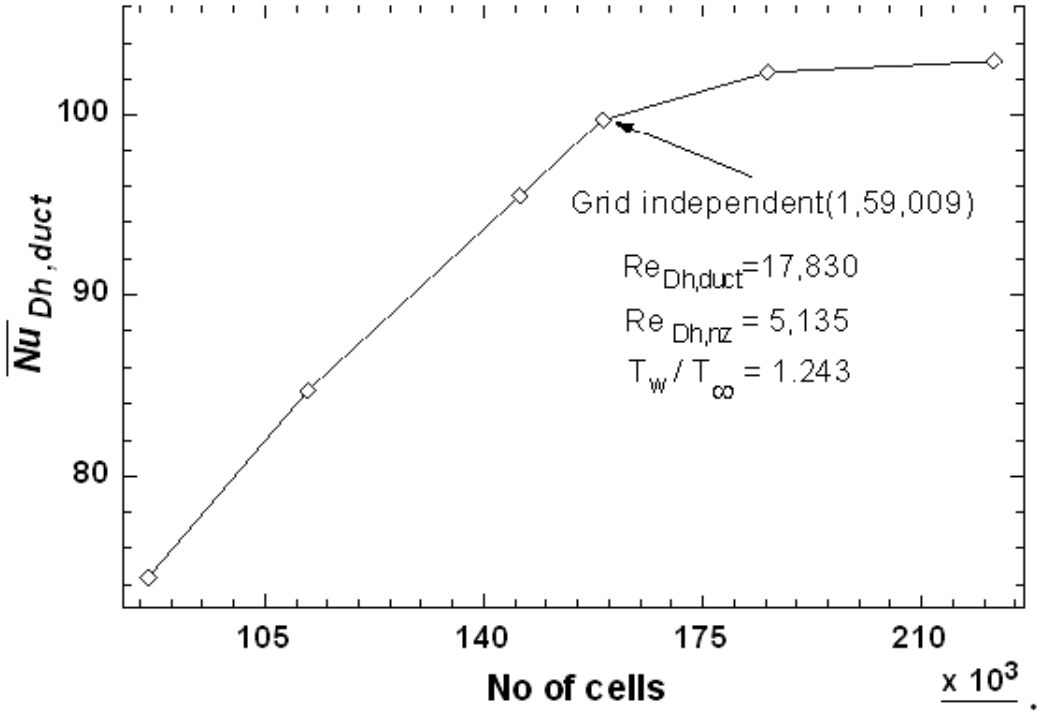

Figure 3: Variation of Nusselt number with number of cells.

5.2. Effect of duct Reynolds number on Nusselt number

Fig. 4(a) shows the variation of Nusselt number with duct Reynolds number ($Re_{Dh,duct}$) as a function of Prandtl number (Pr) of the fluid. For a particular nozzle Reynolds number ($Re_{Dh,nz}$), it has been seen that Nusselt number increases monotonously with duct Reynolds number. For example, at Pr = 0.7, the Nusselt number has been enhanced by 92.45% as $Re_{Dh,duct}$ is increased from 17,900 to 53,900. The enhancement in the Nusselt number is even more at high Prandtl number fluids. In case of high Prandtl number fluids, the specific heat of the fluid becomes more and the high specific heat can able to carry more heat from the heated surface so as to obtain a higher Nusselt number. The expanded and cutaway view of the temperature contours in X-Y plane passing through the mid-width of the duct has been shown in Fig. 4(b) and (c). As it can be seen from Fig. 4(a), the high value of Prandtl number (Pr = 15) maintains a uniform temperature near the heated surface. The thermal boundary

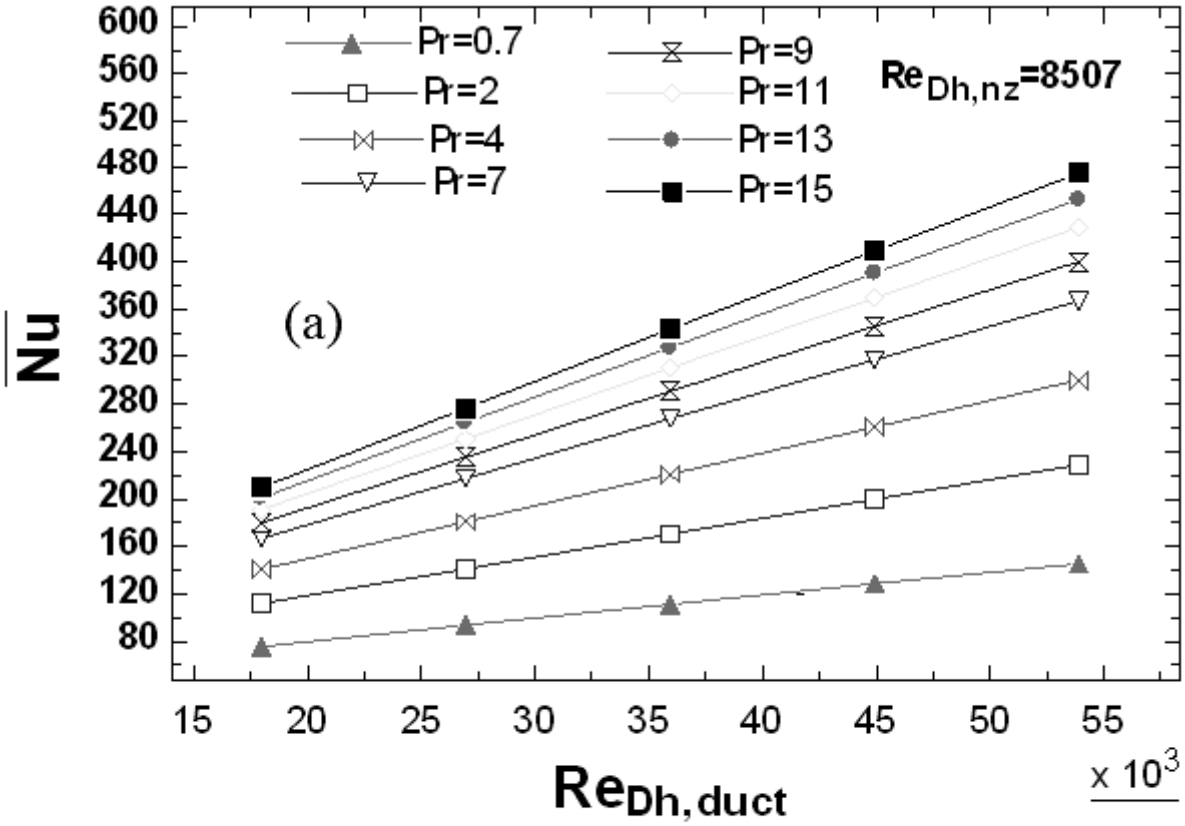

(a)

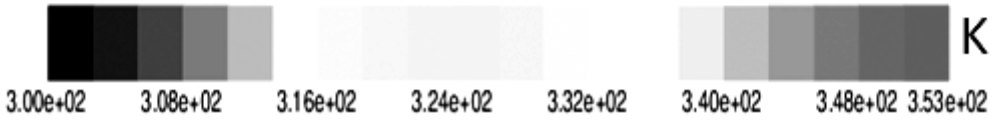

(b)

Figure 4. (a) Variation of Nusselt number with duct Reynolds number as function of Prandtl number of the fluid; expanded and cutaway view of (b) temperature contour for Pr = 15 (c) temperature contour for Pr = 0.7.

layer in the vicinity of the wall has been weakened. However, at low Prandtl number (Pr = 0.7), a distinct and thicker thermal boundary layer has been observed (see Fig. 4(c)), which restricts the transfer of heat from the heated solid wall to the bulk fluid leading to a lower Nusselt number.

5.3. Effect of nozzle Reynolds number on Nusselt number

Figure 5 shows the effect of the nozzle Reynolds number on the area weighted average Nusselt number at different duct Reynolds number. The increment in the Nusselt number with the nozzle Reynolds number is found to be insignificant. Thus, these variations are almost flat with the nozzle Reynolds number.

As the considered range of nozzle Reynolds number ($3,400 \le \mathrm{Re}_{Dh,nz} \le 10,200$) is lower than the considered range for the duct Reynolds number ($17,900 \le \mathrm{Re}_{Dh,duct} \le 53,900$), the flow, after emanating from the nozzle exit is blow away with the oncoming high momentum fluid from the duct inlet. Thus, the nozzle fluid although imparts mixing of the hot and cold fluid, but it is not impinged directly on the heated surface leading to a flat variation in Nusselt number.

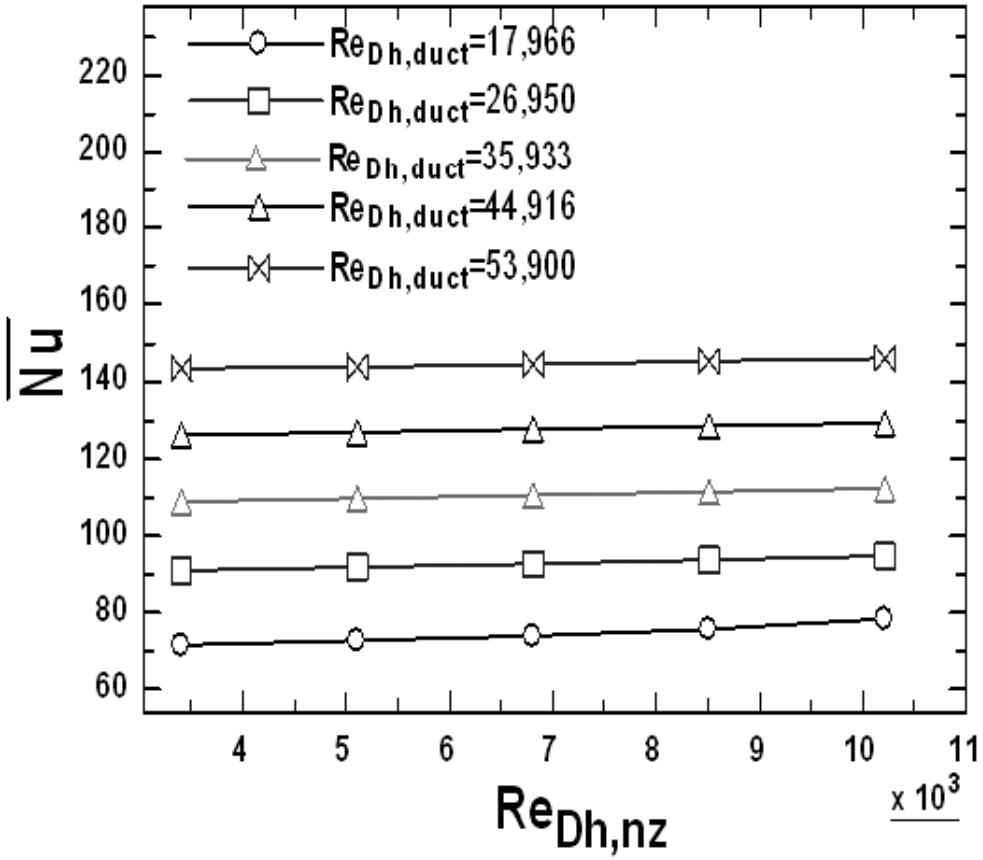

Figure 5: Variation of Nusselt number with nozzle Reynolds number as function of duct Reynolds number

5.4. Effect of duct Reynolds number on pressure drop as a function of Nozzle Reynolds number

The variations of pressure drop and pumping power with the duct Reynolds number are shown in Figs. 6(a) and (b), respectively. As it is expected, the pressure drop increases both with the duct as well as nozzle Reynolds number. The pumping power for the present investigation has been computed as follows:

$$PP = \forall \times \Delta P \tag{16}$$

Where $\forall$ is the volume flow rate (m^3/s)

The pressure drop is increases with the Reynolds number, and thus the pumping power () increases with duct Reynolds number because of the direct dependency of the pumping power on the pressure drop.

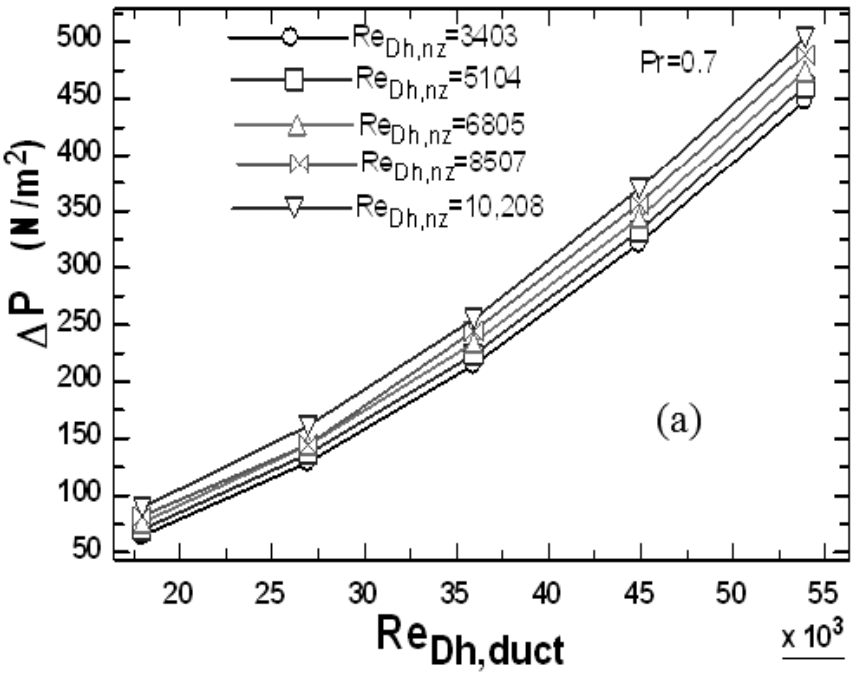

(a)

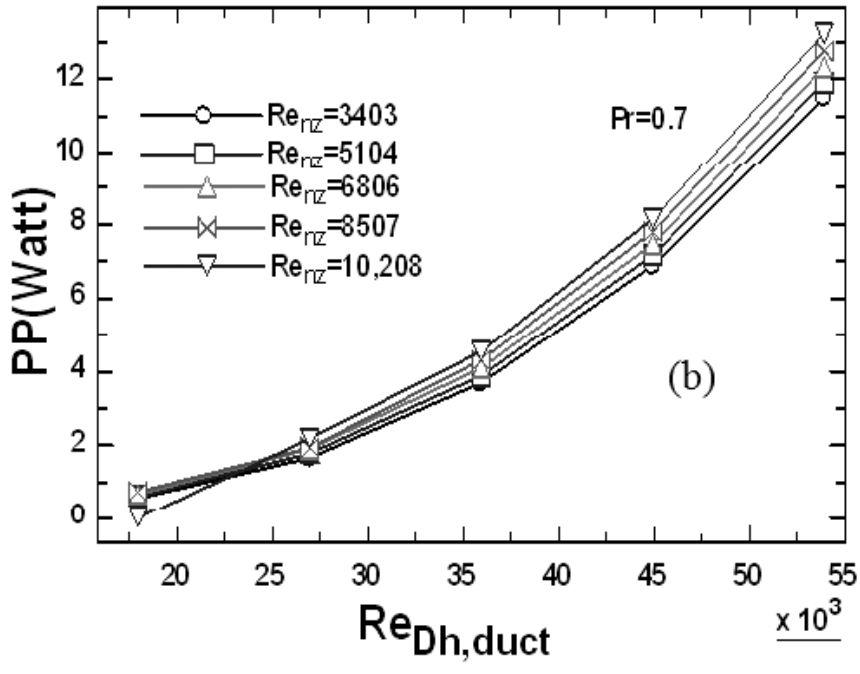

(b)

Figure 6: (a) Pressure drop variation with duct Reynolds number; b) pumping power variation with duct Reynolds number

6. CONCLUSIONS

Governing equations for mass, momentum and energy have been solved in a 3-D computational domain using the commercial code ANSYS Fluent 16. The heat transfer rate for a protruded surface has been computed by capturing the Nusselt number. Following conclusion are made from this study:

1. The duct Reynolds number is found to be best parameter for the heat transfer enhancement in cross-flow cooling strategies. It is observed that the average Nusselt number is increased with the duct Reynolds number and Prandtl number.
2. The Nusselt Number varies insignificantly with the nozzle Reynolds number, since the flow is expected to be blown away with the high momentum incoming duct flow. However, a strong variation in the Nusselt number with the duct Reynolds number has been observed at a particular nozzle Reynolds number.
3. The pressure drop, and so the pumping power are increased with the duct Reynolds number.

NOMENCLATURE

k	Turbulent kinetic energy (m^2/s^2)
$\overline{Nu}_{Dh,Duct}$	Average Nusselt number
$Re_{(Dh,Duct)}$	Reynolds number based on hydraulic diameter of duct
$Re_{(Dh,Nz)}$	Reynolds number based on hydraulic diameter of nozzle
T_∞	Ambient temperature (K)
T_w	Isothermal wall temperature (K)
u_{in}	Velocity at duct inlet (m/s)
Q	Heat flux of isothermal surface (W/m2)
$\forall$	Total volume flow rate (m3/s)
x	Axial direction along isothermal surface

Greek letters

Δp	Pressure drop (N/m^2)
k	Thermal conductivity (W/m-K)
μ	Dynamic viscosity of fluid (kg/m-s)
p	Fluid density (kg/m^3)
ω	Specific dissipation rate (1/s)

Subscripts

N_z	Nozzle
D_h	Hydraulic diameter
w	Wall
∞	Ambient

REFERENCES

[1] Mudawar, Assessment of high-heat-flux thermal management schemes, Proc. Seventh Intersoc. Conf. Therm. Therm. Mech. Phenom. Electron. Syst. 1 (2000) 1-20.

[2] L.T. Yeh, Review of heat transfer technologies in electronic equipment, ASME J. Electron. Packag. 117 (1995) 333-339.

[3] Dewan, P. Patro, I. Khan, P. Mahanta, The effect of fin spacing and material on the performance of a heat sink with circular pin fins, J. Power Energy 224 (2010) 35-46.

[4] B.N. Prasad, J.S. Saini, Effect of artificial roughness on heat transfer and friction factor in a solar air heater, Sol. Energy 41 (1988) 555-560.

[5] D. Gupta, S.C. Solanki, J.S. Saini, Heat and fluid flow in rectangular solar air heater duct having transverse rib roughness on absorber plates, Sol. Energy 51 (1993) 31-37.

[6] A. Lanjewar, J.L. Bhagoria, R.M. Sarviya, Heat transfer and friction in solar air heater duct with W-shaped rib roughness on absorber plate, Energy 36 (2011) 4531-4541.

[7] A.M. Ebrahim Momin, J. Saini, S. Solanki, Heat transfer and friction in solar air heater duct with V-shaped rib roughness on absorber plate, Int. J. Heat Mass Transf. 45 (2002) 3383-3396.

[8] R. Karwa, B.K. Maheshwari, N. Karwa, Experimental study of heat transfer enhancement in an asymmetrically heated rectangular duct with perforated baffles, Int. Commun. Heat Mass Transf. 32 (2005) 275-284.

[9] R. Karwa, B.K. Maheshwari, Heat transfer and friction in an asymmetrically heated rectangular duct with half and fully perforated baffles at different pitches, Int. Commun. Heat Mass Transf. 36 (2009) 264-268.

[10] M.M.K. Bhuiya, M.S.U. Chowdhury, M.T. Saha, Islam heat transfer and friction factor characteristics in turbulent flow through a tube fitted with perforated twisted tape inserts, Int. Commun. Heat Mass Transf. 46 (2013) 49-57.

[11] T. Alam, R.P. Saini, J.S. Saini, Experimental investigation on heat transfer enhancement due to V-shaped perforated blocks in a rectangular duct of solar air heater, Energy Convers. Manage. 81 (2014) 374-383.

[12] G. Zhou, Z. Feng, Experimental investigations of heat transfer enhancement by plane and curved winglet type vortex generators with punched holes, Int. J. Therm. Sci. 78 (2014) 26-35.

[13] J. Sakakibara, K. Hishida, M. Maeda, Vortex structure and heat transfer in the stagnation region of an impinging plane jet, Int. J. Heat Mass Transf. 40 (1997) 3163-3176.

[14] R. Gardon, J.C. Akfirat, The role of turbulence in determining the heat transfer characteristics of impinging jets, Int. J. Heat Mass Transf. 8 (1965) 1261-1272.

[15] N. Didden, C.M. Ho, Unsteady separation in a boundary layer produced by an impinging jet, J. Fluid Mech.

[16] A. K. Barik ,S. Rout ,A. Mukherjee , Numerical investigation on heat transfer enhancement from a protruded surface by cross-flow jet using Al_2O_3-Water nanofluid, International journal of heat and mass transfer , Vol. 101(2016) pp. 550-551.

[17] F.R. Mentor, Two-equation eddy-viscosity turbulence models for engineering applications, AIAA J. 32 (1994) 1598–1605.

[18] A. K. Barik, A. Mukherjee, and P. Patro, "Heat transfer enhancement for a small rectangular channel with different surface protrusions by a turbulent cross flow jet*". Int. J. of Therm Sci*. 98,2015,pp.32-41

[19] B. E. Launder, D. B. Spalding, The numerical computation of turbulent flows, Comput. Methods Appl. Mech. Eng. 3 (1974) 269–2879.

[20] A. K. Barik, S. K. Dash, A. Guha, Experimental and numerical investigation of air entrainment into an infrared suppression device, Appl. Therm. Eng. 75 (2015) 33–44.

[21] A. K. Barik, S. K. Dash, A. Guha, New correlation for prediction of air entrainment into an Infrared Suppression (IRS) device, Appl. Ocean Res. 47 (2014) 303–312.

[22] A. K. Barik, S. K. Dash, A. Guha, Entrainment of air into an infrared suppression (IRS) device using circular and non-circular multiple nozzles, Comput. Fluids 114 (2015) 26–38.60 (1985) 235-256.

[23] C. A. Slicher, M.W. Rouse, A convenient correlation for heat transfer to constant and variable property fluids in turbulent pipe flow, Int. J. Heat Mass Transf. 18 (1975) 677e683.

[24] S. Kakac, R.K. Shah, W. Aung, Handbook of Single-phase Convective Heat Transfer, John Wiley and Sons, New York, 1987.